16th ICAAR LISBOA 2020-2022

16th International Conference on
Alkali-Aggregate Reaction in Concrete
Lisboa | LNEC | Portugal | 31 May - 2 June 2022

http://icaar2020-2022.lnec.pt

Numerical simulation of concrete swelling using mesoscale detailed 2D particle models taking into account aging viscoelasticity and damage

Carlos Serra [(1)], Nuno Monteiro Azevedo [(2)], António Lopes Batista [(3)]

(1) *Laboratório Nacional de Engenharia Civil, Lisboa, Portugal, cserra@lnec.pt*

(2) Laboratório Nacional de Engenharia Civil, Lisboa, Portugal, nazevedo@lnec.pt

(3) Laboratório Nacional de Engenharia Civil, Lisboa, Portugal, albatista@lnec.pt

Abstract

Concrete swelling due to internal expansion reactions (IER) concerns both physical and chemical phenomena which can have strong interactions as the swelling process evolves. Modelling the effects of swelling on the mechanical behaviour of concrete is of the most importance in order to predict the development of the deterioration, to assess structural safety and to determine the efficiency of rehabilitation techniques to reduce the negative impact of swelling.

Mesoscale models are being used for the study of the behaviour of concrete focusing on the interactions between aggregates and the maturing cement paste in order to evaluate development of the main mechanical properties. These types of models are particularly relevant for the study of swelling since the aggregate structure of concrete and the interfacial transition zone (ITZ) are explicitly taken into account.

This paper refers to the numerical simulation of concrete swelling using detailed 2D particle models in which the particles representing the coarse aggregates and the binding mortar define the concrete mesostructure. In the particle model, swelling is represented by a change in the normal contact force due to a change in the inter-particle relative displacement caused by the progressive particle area growth. Since the swelling reactions occur relatively slow over a large period of time, creep and relaxation properties of concrete are taken into account. The paper evaluates the effect of aging viscoelasticity on the development of stress inside the concrete and for predicting the progress of damage over time.

Keywords: *Mesoscale modelling, Particle models, Swelling, Creep, Damage*

1. INTRODUCTION

At the mesoscale, the main structural heterogeneity in concrete is due to the presence of aggregates, mainly because of the differences between the mechanical properties of the particles representing the aggregate and particles representing the cement paste and due to the weaker properties of the interfacial transition zone (ITZ). Mesoscale analyses are being used to study the behaviour of concrete focusing on the interactions between coarse aggregates and the maturing mortar in order to evaluate the main mechanical properties and their development over time. It is known that stiff aggregates restrain the deformations, introducing a non-uniform stress field inside concrete in which there are highly stressed areas. Creep has a significant role in the relaxation of these stresses and in the progress of damage, namely due to swelling reactions, which occur relatively slow over time [1–3].

The representation of the mesostructure of concrete allows for a more detailed research of specific phenomena, such as the coupling between creep and damage in which the physical explanation takes place at the mesoscale [4], the development of internal self-balanced stresses that occur during hydration and hardening of concrete [5, 6] and the study of stress development on concrete affected by alkali-silica reactions [3]. Mesoscale analyses are particularly relevant for the study of internal expansion reactions (IER) since the aggregate structure of concrete and the interfacial transition zone (ITZ) are explicitly taken into account [7]. Some numerical work has been done considering the interaction between creep and damage at the mesoscale [3] and in a practical application at the macroscale [8, 9], for the concrete swelling simulation.

The use of discrete or distinct element method (DEM) was first applied to the study of geotechnical materials of granular nature. Cundall described the basis for the DEM simulation by considering the movement and interaction of rock blocks [10] and of 2D circular elements [11]. Later on, cracking was taken into account for geomaterials, such as rock, with very simple contact models between rigid elements [12, 13]. Particle models applied to DEM are especially suited for the analysis of quasi-brittle behaviour of some heterogeneous materials, such as concrete, since it is easier to consider the material microstruture and the randomness of material heterogeneity [14] and due to its computational simplicity, when compared with finite element method formulations. A detailed DEM particle model including the particles representing the mortar allows for the contact constitutive models to be less complex when compared with lattice models that do not have the same degree of discretization [15, 16].

This paper shows the implementation of a swelling contact model on an established numerical tool for the study of long-term aging viscoelastic behaviour of plain concrete at the mesoscale [17], using 2D particle models. The main goals are to verify the model and do a preliminary parametric study on the effects of aging viscoelasticity and damage for three different types of swelling and for each type of component of concrete, namely the binding mortar, the aggregates and the ITZ. A reference case from previous work [17] is used to compare the effects of aging viscoelasticity and damage and understand the force distribution inside concrete over time for specific swelling scenarios.

2. DISCRETE ELEMENT METHOD FORMULATION AND CONSTITUTIVE MODELS

2.1 Discrete element method based on particle models

The discrete element method (DEM) can be described as a numerical method for solving structural systems of individual elements, blocks (polygons) or particles (circular or spherical) interacting with each other at contact points or interfaces. Each element, usually considered to be rigid, is ruled by a motion law and each contact by an interaction law.
The Newton's second law of motion defines the differential equation that governs the kinematics of the elements, which is solved using explicit methods. The interaction law determines the interaction forces between elements at the contact point, according to their relative displacement. In the adopted DEM particle model, the elements interacting with each other are circular rigid particles defined by a position in space and a given radius.
The normal and shear contact force increments, ΔF_n and $\Delta \boldsymbol{F}_s$, are obtained from an incremental linear constitutive law of the contact,

$$\Delta F_n = -k_n \Delta x_n , \qquad \Delta \boldsymbol{F}_s = -k_s \Delta x_s \tag{1}$$

where Δx_n and $\Delta \boldsymbol{x}_s$ are the normal and shear contact displacement increments, respectively, and k_n and k_s are the normal and shear contact stiffnesses.
The mechanical critical time step, related to the maximum frequency and required for explicit time integration schemes, is usually very small, which can be time consuming and computationally demanding. In order to avoid overshooting of the solution, an adaptive dynamic relaxation algorithm (ADR) can be used in which the global damping coefficient is updated at each time increment [18]. At each step, the scaled masses and inertias need to be updated for stability purposes whenever there is a change in the model stiffness, for example due to the constitutive law, to damage or if new contacts are found to occur during the numerical simulation.

2.2 Aging viscoelastic contact model based on the solidification theory

The aging viscoelastic model used is based on Bažant's solidification theory [5]. The model considers the viscoelastic strain, ε_v, a consequence of the volume fraction growth associated to the viscoelastic behaviour, $v(t)$, and the viscous strain, ε_f, a consequence of the volume fraction growth associated with the viscous behaviour, $h(t)$, and has a consistent mathematical formulation.
One can write the quasi-elastic incremental contact normal force, ΔF_n, as follows,

$$\Delta F_n = k_n''(\Delta x_n - \Delta x_n'') \tag{2}$$

$$\frac{1}{k_n''} = q_{1,n} + \frac{1}{v_n(t_i^*)}\sum_{\mu=0}^{N}\left(\frac{1-\lambda_{\mu,n}}{k_{\mu,n}}\right), \Delta x_n'' = \frac{\Delta\gamma_n''}{v_n(t_i^*)} + \frac{q_{4,n}F_n(t_i^*)\Delta t_i}{t_i^*} \tag{3}$$

$$v_n(t) = \left(\frac{1}{t}\right)^m + \frac{q_{3,n}}{q_{2,n}} \tag{4}$$

The shear contact behaviour follows the same formulation as the one previously described for the normal direction.
To simulate the creep behaviour of structural systems, such as rock or concrete, the total calculation time can be expensive. A fast numerical procedure for the long-term behaviour was adapted for cementitious materials and makes use of the adaptive dynamic relaxation method to obtain a fast equilibrium without overshooting, considering the aging viscoelastic contact model [17].

2.3 Swelling contact model

Assuming that the swelling reactions occur in an isotropic material with elastic behaviour, the free swelling increment due to a chemical reaction within a close system can be expressed by a differential equation, see [19], defined in equation (5).

$$t_C(T,\xi)\frac{d\xi}{dt} + \xi = 1 \tag{5}$$

In which,

$$t_C(T,\xi) = \tau_C(T)\frac{1 + e^{[-\tau_L(T)/\tau_C(T)]}}{\xi + e^{[-\tau_L(T)/\tau_C(T)]}} \tag{6}$$

$$\xi = \frac{\varepsilon_{swelling}(t)}{\varepsilon_{swelling}(t=\infty)} \tag{7}$$

and $\varepsilon_{swelling}(t)$ is the swelling strain over time, $\varepsilon_{swelling}(t=\infty)$ is the long-term swelling at infinite time, τ_L is the latency time, τ_C is the characteristic time and T is the temperature.

The solution of the differential equation (5) is a sigmoid function,

$$\varepsilon_{swelling}(t) = \varepsilon_{swelling}(t=\infty)\frac{1 - e^{[-t/\tau_C]}}{1 + e^{[-(t-\tau_L)/\tau_C]}} \tag{8}$$

The swelling contact model, at constant temperature, is based on the previous sigmoid function, adapted to define a normal displacement increment representing relative displacement caused by the swelling of two particles in contact, $\Delta x_{n,swelling}$, considering an equivalent maximum normal displacement at infinite time, $d_{swelling}(t=\infty)$, and the respective latency time and characteristic time, τ_L^* and τ_C^*.

$$\Delta x_{n,swelling}(t) = d_{swelling}(t=\infty)\left(\frac{1 - e^{[-t_i/\tau_C^*]}}{1 + e^{[-(t_i-\tau_L^*)/\tau_C^*]}} - \frac{1 - e^{[-t_{i-1}/\tau_C^*]}}{1 + e^{[-(t_{i-1}-\tau_L^*)/\tau_C^*]}}\right) \tag{9}$$

The constitutive contact model, including the swelling normal displacements, is updated from equation (2) to,

$$\Delta F_n = k_n''\left(\Delta x_n - \Delta x_n'' + \Delta x_{n,swelling}\right) \tag{10}$$

2.4 Damage contact model

A Mohr-Coulomb model with a tension cut-off (brittle model) is adopted at the contact level. The tensile force of each contact i, $F_{n,max,contact\,i}$. is limited by a maximum tensile normal strength of the corresponding material. The force-displacement model in the normal direction is brittle for tensile forces.

Until the normal contact force and the shear force is below their maximum values, the contact is elastic. Once one of the failure conditions is met, the contact breaks and behaves as a Mohr-Coulomb model with null cohesion for the shear sliding at the contact and the contact only bears compressive forces.

3. NUMERICAL TESTS FOR THE SIMULATION OF DIFFERENT SWELLING PROCESSES IN CONCRETE

3.1 General aspects

This section presents a set of numerical tests focused on studying the effect of aging viscoelasticity and damage in swelling processes in concrete at a mesoscale, considering the concrete's heterogeneity, namely binding mortar, aggregates and ITZ. The simulation of cementitious materials using particle models imply the use of assemblies that represent the main characteristics of each material. The mortar and the coarse aggregates will be considered as uniform materials with specific deformability properties. In order to have comparable results, it will be used a concrete particle model which has already been studied in previous works [17]. The micro parameters of the aging viscoelastic contact model were calibrated to fit the experimental results of Ward [20] and the mechanical properties of ITZ contacts were determined.

The study includes the analysis of three types of concrete swelling, internal sulphate reaction (ISR), alkali-silica reaction considering reactive fine aggregates (ASR-fine agg.) and alkali-silica reaction considering reactive coarse aggregates (ASR-coarse agg.), occuring in different time scales. ISR, due to time delayed ettringite formation, usually occurs within the first years after casting, whereas ASR exhibits a behaviour characterized by very low expansion rates during the first years but develops over several decades. Generic mean parameters were adopted for each type of reaction (§3.2). It is assumed that ISR type causes swelling in the binding mortar and in the ITZ (as ettringite progressively fills the ITZ) [21] and ASR-fine agg. reactions occur only in the binding mortar, while swelling due to ASR-coarse agg. type reactions originates from small areas of the aggregate, gel pockets (inside and near the boundary), as described in the literature [2, 22, 23].

Firstly, the proposed swelling contact model is validated considering a single contact and a random assembly for the mortar/ITZ. A generic description of the procedure for the creation of compact particle assemblies and of concrete's aggregate structure is presented, as well as the deformability properties of the concrete components, based on a calibration of B3 model coefficients.

The two final sections show the numerical results of each type of analysis, considering, separately, the effect of aging viscoelasticity of the binding mortar and ITZ and the effect of damage of each component, including the aggregate.

3.2 Swelling contact model validation and calibration of micro parameter

Table 3.1 presents the validation of the proposed swelling contact model for a two particle-one contact assembly, in which the swelling contact displacements, $d_{swelling}$, can be directly related to the swelling strains, $\varepsilon_{swelling}$. It also presents the parameter values used in the study for each type of analysis. Figure 3.1 shows the accuracy of the fast numerical procedure for the long-term and swelling behaviour considering different timesteps, N (N=2, 5, 10 and 20), equally spaced in log-scale.

Table 3.1: Validation of swelling contact model

Type of assembly	Material	$d_{swelling}$ $(t = \infty)$ (×10⁻⁶ m)	ISR type analysis			ASR-fine agg. type analysis ASR-coarse agg. type analysis		
			τ_C (days)	τ_L (days)	$\varepsilon_{swelling}$ $(t = 3650\ days)$ (×10⁻⁶)	τ_C (days)	τ_L (days)	$\varepsilon_{swelling}$ $(t = 50000\ days)$ (×10⁻⁶)
2 × 1	-	1000	50	100	1000	2500	5000	1000

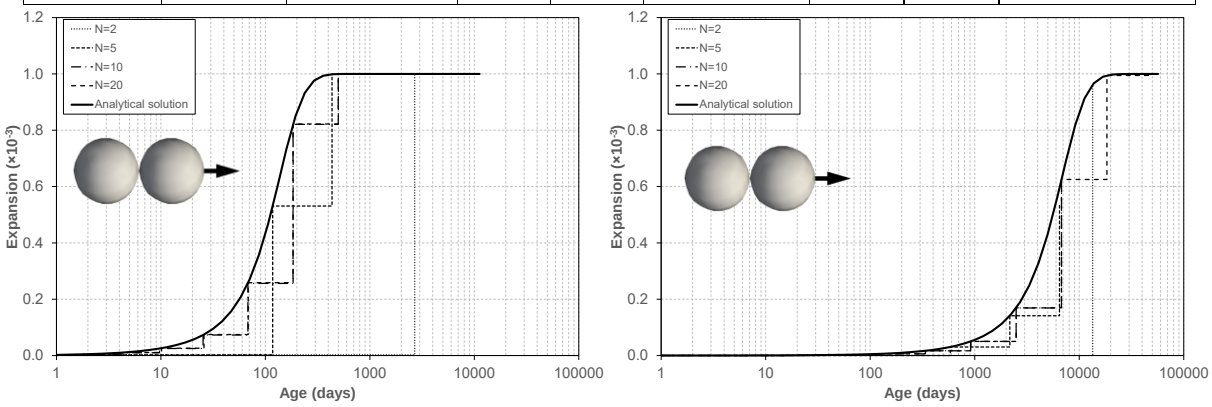

Figure 3.1: Validation of the swelling contact model for a 2 × 1 particle assembly: a) ISR type analysis; b) ASR type analysis

To reproduce the macroscopic behaviour of each swelling material, the micro parameter, $d_{swelling}(t = \infty)$ for the swelling contact model of mortar and ITZ, was determined for a predefined ultimate macroscopic swelling strain, $\varepsilon_{swelling}(t = \infty) = 1000 \times 10^{-6}$. Table 3.2 shows that the adopted micro-macro relation $d_{swelling}(t = \infty) = \varepsilon_{swelling}(t = \infty) \times 2\ R_{mean}$ gives a reasonable approximation, in which R_{mean} is the mean radius of the random particle assembly (Table 3.2).

Table 3.2: Calibration of swelling contact micro parameters

Type of assembly	Material	$d_{swelling}$ $(t = \infty)$ (×10⁻⁶ m)	ISR type analysis			ASR-fine agg. type analysis		
			τ_C (days)	τ_L (days)	$\varepsilon_{swelling}$ $(t = 3650\ days)$ (×10⁻⁶)	τ_C (days)	τ_L (days)	$\varepsilon_{swelling}$ $(t = 50000\ days)$ (×10⁻⁶)
Random $(R_{max} = 0.48\ mm$ $R_{min}/R_{max} = 2/3$ $R_{mean} = 0.397\ mm)$	Mortar / ITZ	$\varepsilon_{swelling}(t = \infty)$ × 2 R_{mean} = 1000 × 2 × 0.000397 = 0.794	50	100	1061	2500	5000	1061

3.3 Generation of compact particle assemblies and of concrete aggregate structure

The aggregate particle assembly is created by first inserting the aggregate particles from the largest diameter to smallest sieve diameter ensuring that the particles do not overlap with each other. The particle assembly of concrete includes the shape, aspect ratio and distribution of the coarse aggregates according to [24]. The particles inside the aggregates are placed in polygonal contour, generated according to the aggregate size and distribution [14]. The aggregate generation procedure allows for the definition of an arbitrary aggregate distribution, which, in this particular case, follows the properties of the tested concrete including the two types of aggregates, 2.4-4.75 mm and 4.75-10 mm, and the proportion of each one in the concrete mix. Later the outer boundary of the aggregate particles is discretized with particles representing the particle distribution adopted for the binding mortar.

The size of the particles used for the simulation has to take into account the concrete mesostructure. It should be small enough to represent the contribution of the smallest aggregate in the concrete behaviour

maintaining a reasonable computational cost. The maximum particle radius was considered to be one fifth of the minimum size of the coarse sand, ϕ_{min}^{agg} ($R_{max} = \phi_{min}^{agg}/5 = 2.4/5 = 0.48\,mm$). The ratio between the minimum and the maximum particle radius, R_{min} and R_{max}, was considered to be two thirds, in order to obtain a compact assembly, similarly to the mortar and ITZ calibration model (§3.2, Table 3.2).

3.4 Mortar, aggregate, ITZ and concrete deformability properties

As mentioned, previous work [17] determined the micro parameters, q_i*, of each component of concrete, which characterizes the aging viscoelastic behaviour of concrete used by Ward [20]. The aging viscoelastic model used to represent the long-term behaviour of concrete was B3 model [25].

Table 3.3 presents the B3 model coefficients of each concrete component, mortar, concrete and ITZ and Figure 3.2 shows the development of the elastic modulus over time, $E(t)$, and the creep compliance for different loading ages, $J(t,t')$. As expected and inferred by other authors, ITZ has much higher creep compliance values than the mortar, which implies lower elastic modulus and higher creep strains over time.

Table 3.3: B3 model coefficients of mortar, concrete and ITZ

Material	q_1* (×10^{-6}/MPa)	q_2* (×10^{-6}/MPa)	q_3* (×10^{-6}/MPa)	q_4* (×10^{-6}/MPa)
Mortar M6	6.7	108.1	44.2	14.3
Concrete C4	9.0	23.7	46.6	5.1
ITZ	19.3	194.6	72.9	7.5

* Estimates obtained from the work developed in [17]

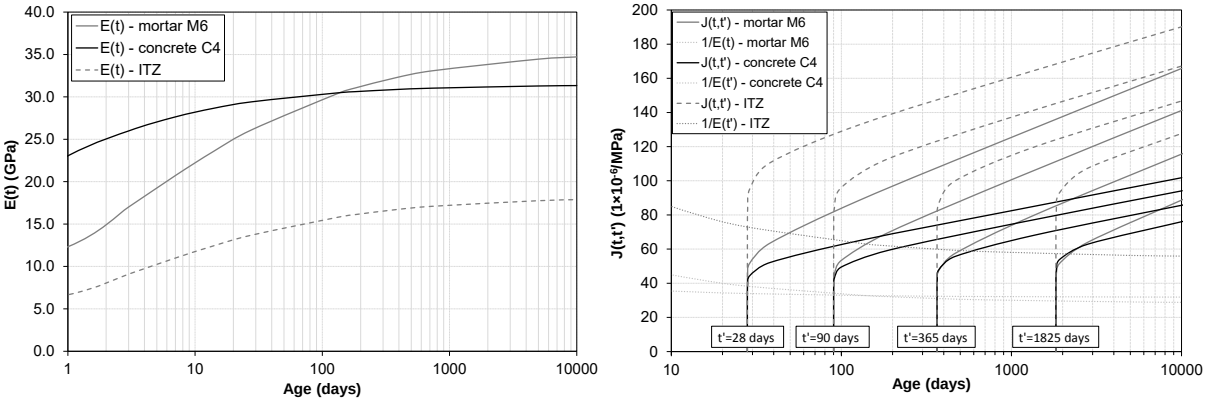

Figure 3.2: Modulus of elasticity and creep compliance of mortar, concrete and ITZ

3.5 Concrete numerical swelling tests considering aging viscoelastic behaviour

3.5.1 Effects of aging viscoelastic behaviour on the swelling development of the concrete specimen

This section describes the results of numerical tests focused on the effect of the aging viscoelastic behaviour on the development of contact forces inside a concrete specimen, for two types of swelling, ISR type and ASR type. Firstly, Figures 3.3, 3.4 and 3.5 show the unbalanced total force during the numerical test and the convergence to equilibrium of the solution for each timestep (left) and the total swelling strains, measured in one direction, over time for each analysis type, ISR, ASR-fine agg. and ASR-coarse agg, considering the input micro parameters and coefficients defined in the Tables 3.2 and 3.3. For the case of ASR-coarse agg. analysis type, it was considered that only 10% of the coarse aggregates contacts had swelling. The results show that, for elastic and viscoelastic behaviour, without damage, the total swelling, after convergence yields lower values than the one observed from plain mortar (1000×10^{-6}), due to aggregate constraint. The particular case of ASR-coarse analysis shows very

little total swelling, since its micro swelling is localized in very small areas inside the aggregates. The viscoelastic effect on the total swelling is very small.

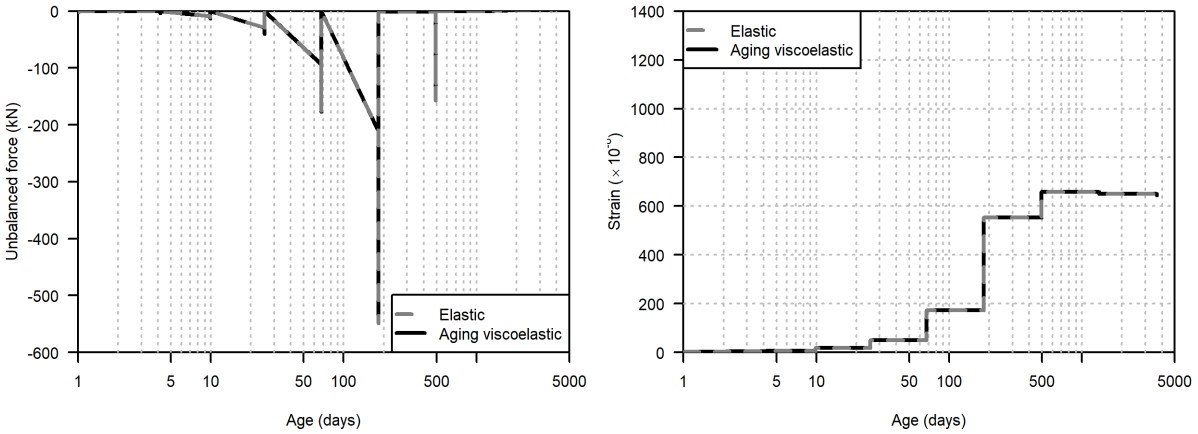

Figure 3.3: Development of unbalanced force during numerical test (left) and total swelling measured in one direction (right), for the ISR analysis

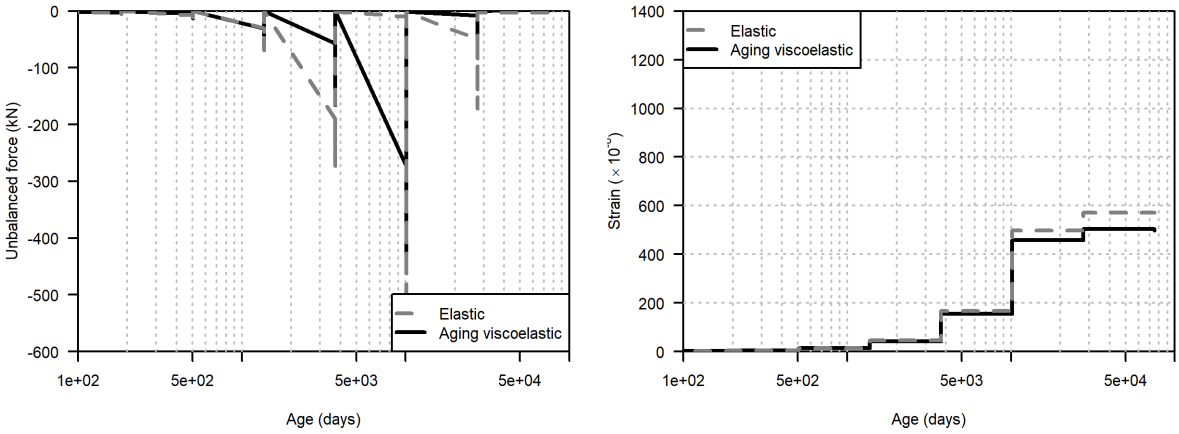

Figure 3.4: Development of unbalanced force during numerical test (left) and total swelling measured in one direction (right), for the ASR-fine agg. analysis

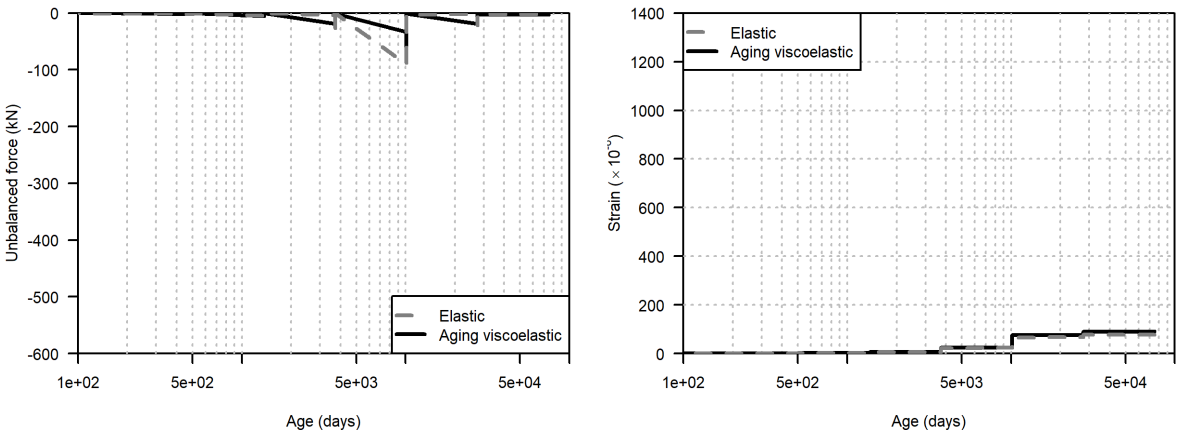

Figure 3.5: Development of unbalanced force during numerical test (left) and total swelling measured in one direction (right), for the ASR-coarse agg. analysis

3.5.2 Effects of aging viscoelastic behaviour on the development of contact forces inside concrete

The different mechanical properties of mortar, ITZ and aggregates have a great influence on the stress heterogeneity inside concrete. The mortar and ITZ stiffness development and the aging viscoelastic behaviour generates a stress transfer from aggregates to the binding mortar over time. The stress distribution is highly dependent of the aggregate structure and the range of coarse aggregate sizes introduces a complex stiff structure in which the forces are drawn to. An accurate physical representation of the stiffness distribution enables a realistic stress localization. Moreover, due to prescribed strains, the effect of aging viscoelasticity of mortar and ITZ leads to stress relaxation, *i.e.* to the decrease of stresses over time.

Figures 3.6, 3.7 and 3.8 present the normal contact forces results of the simulation of a swelling test applied to a concrete particle model, considering the elastic and the aging viscoelastic behaviour of the binding mortar and the ITZ, for the ISR type analysis, for the ASR-fine agg. type analysis and for the ASR-coarse agg. type analysis, respectively. The analysis considering the elastic behaviour of the materials included the development over time of mortar and ITZ modulus of elasticity.

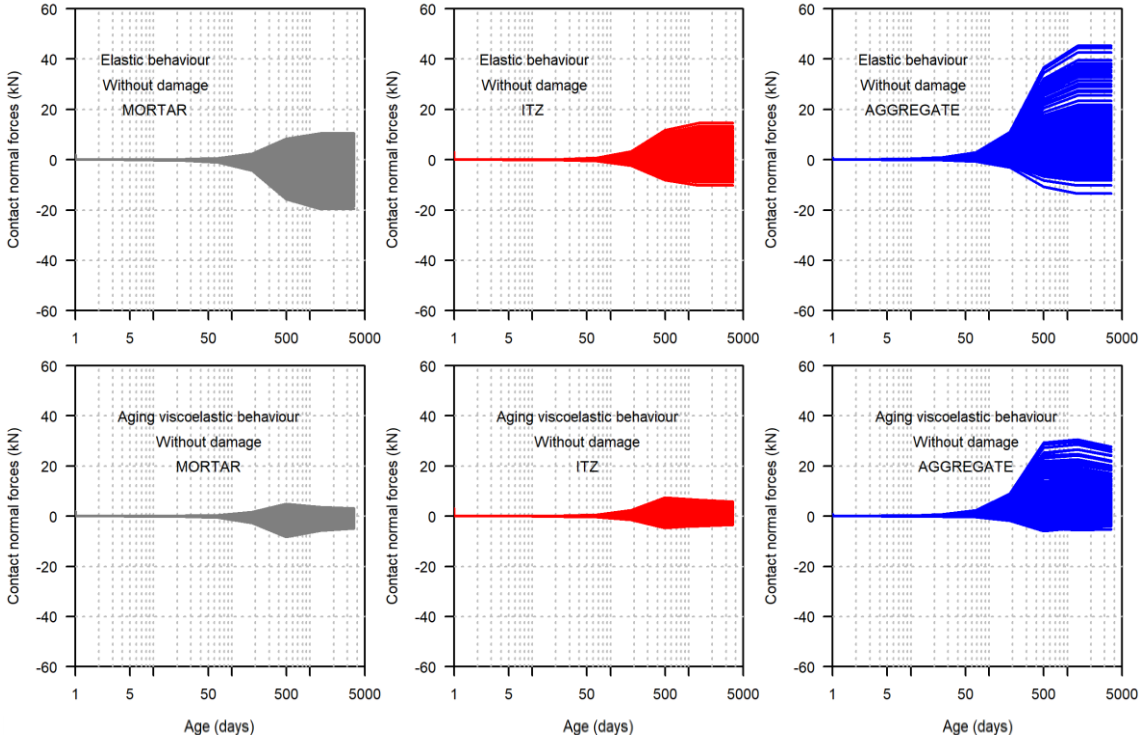

Figure 3.6: ISR type analysis results: Normal contact forces development over time for each type of contact (mortar, ITZ and aggregate) considering elastic behaviour (top) and aging viscoelastic behaviour (bottom)

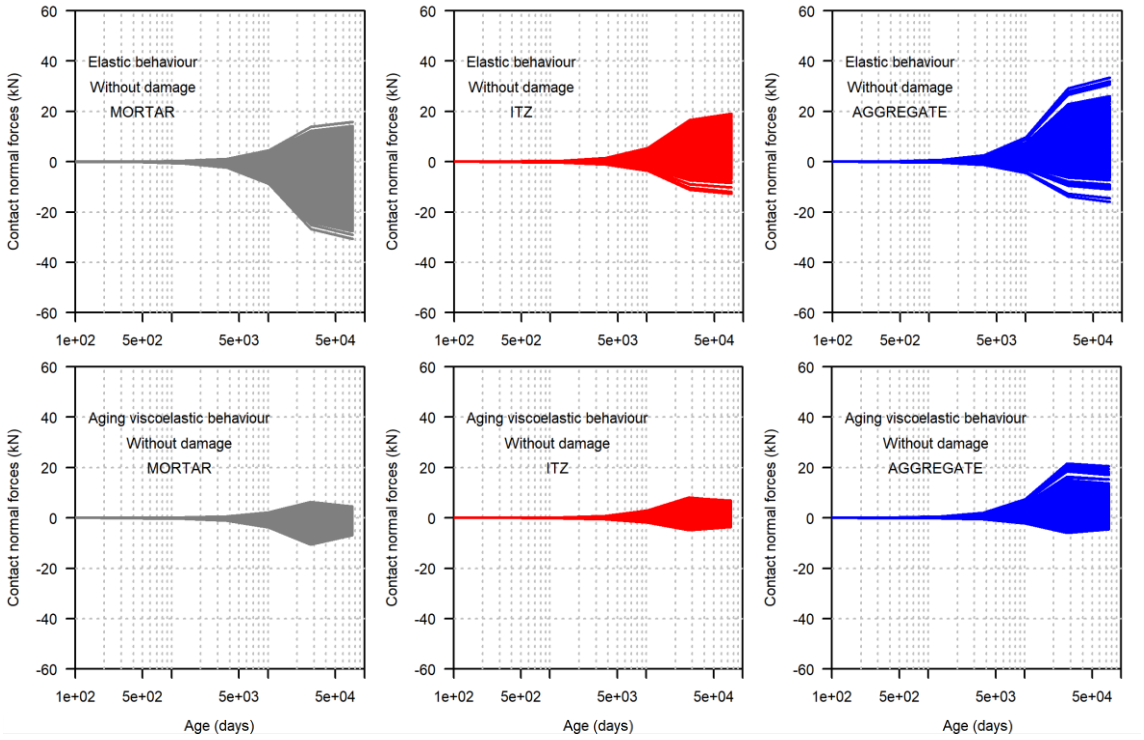

Figure 3.7: ASR-fine agg. type analysis results: Normal contact forces development over time for each type of contact (mortar, ITZ and aggregate) considering elastic behaviour (top) and aging viscoelastic behaviour (bottom)

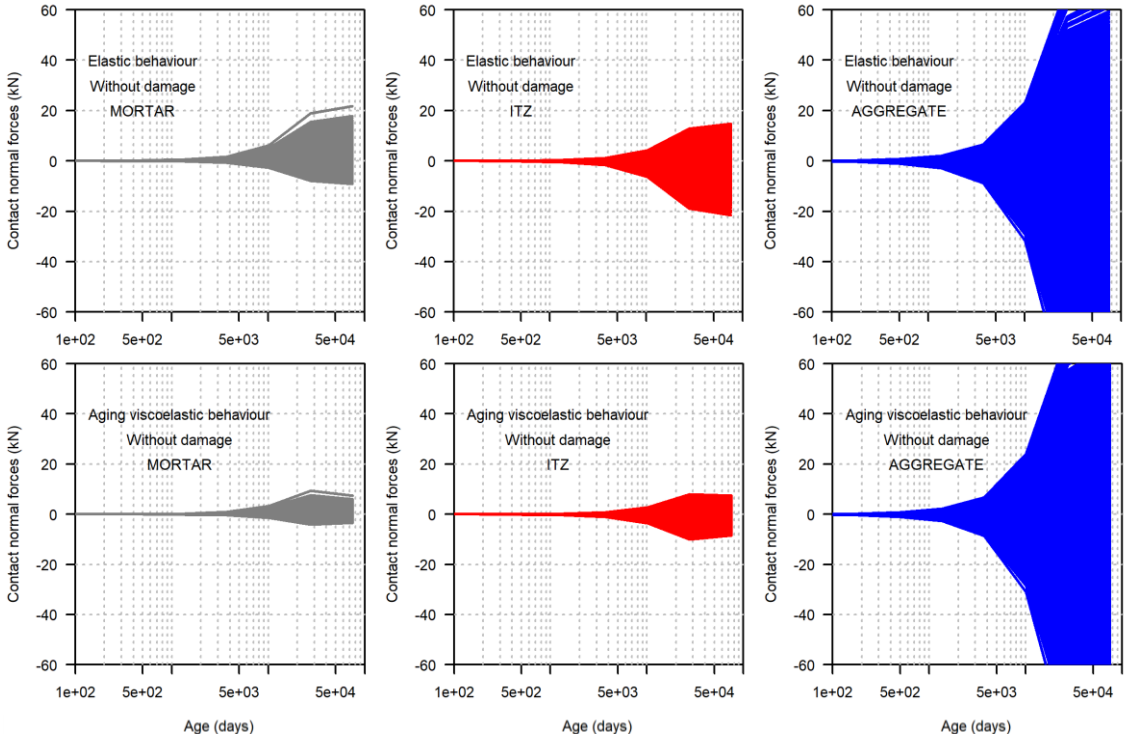

Figure 3.8: ASR-coarse agg. type analysis results: Normal contact forces development over time for each type of contact (mortar, ITZ and aggregate) considering elastic behaviour (top) and aging viscoelastic behaviour (bottom)

Table 3.4 summarizes the results obtained for the last step of the analysis, in which the normal contact forces are higher. Each column refers to the 5% probability values (lowest values, usually in compression) and 95% probability values (highest values, usually in tension) of the distribution of contact

forces considering all the contacts, separated by type of material (mortar, ITZ and aggregate). A comparison between the ISR and ASR results with the elastic results is also presented.

These results allows several conclusions to be drawn, which are in agreement with the expected physical behaviour of swelling concrete:

- For ISR and ASR-fine agg. analysis, mortar contacts are mostly in compression and aggregate contacts are mostly in tension. ITZ contacts have a wider contact force distribution (with several contacts both in tension and in compression);
- The effect of aging viscoelasticity reduces the contact forces of every type of contact, due to force relaxation. The obtained numerical results show that, although the force relaxation only occurs in the mortar and ITZ contacts, the aggregate contacts also show a significant reduction due to force redistribution inside the specimen;
- Higher contact forces were obtained for the ASR type of analysis, considering both elastic and aging viscoelastic behaviour, due to greater stiffness of the binding mortar at later ages;
- The effect of aging viscoelasticity contact behaviour has slightly greater effect on the ISR type analysis, since it occurs in a period of property development over time. This relates with the lower relaxation properties for later ages;
- For ASR-coarse agg. analysis, the internal forces in the aggregates are higher than for the other analysis, since the swelling starts inside the aggregate and the effect of viscoelasticity is lower.

Table 3.4: Summary normal contact forces results of each analysis type

Type of analysis	Type of contact behaviour	Type of material	Normal contact forces (kN) | Variation to reference contact behaviour (%)			
			5%		95%	
ISR	Elastic **(reference)**	MORTAR	-8.3	-	2.5	-
		ITZ	-3.7	-	6.3	-
		AGG	0.0	-	8.4	-
	Aging viscoelastic	MORTAR	-2.0	-76	0.6	-76
		ITZ	-1.6	-57	1.9	-70
		AGG	-0.5	-	3.1	-63
ASR-fine agg.	Elastic **(reference)**	MORTAR	-13.5	-	3.8	-
		ITZ	-1.6	-	0.6	-
		AGG	0.5	-	1.2	-
	Aging viscoelastic	MORTAR	-3.4	-75	1.0	-74
		ITZ	-0.7	-56	3.3	-69
		AGG	-0.2	-140	3.7	-67
ASR-coarse agg.	Elastic **(reference)**	MORTAR	-1.9	-	3.6	-
		ITZ	-8.6	-	4.6	-
		AGG	-55.4	-	30.7	-
	Aging viscoelastic	MORTAR	-0.7	-63	1.1	-69
		ITZ	-3.2	-63	1.9	-59
		AGG	-47.7	-14	31.8	4

3.5.3 Damage development over time due to concrete swelling numerical tests

In this preliminary work damage is only considered in the normal direction, based on the brittle failure of contact. The maximum normal contact force for each contact i, $F_{n,max,contact\ i}$, can be derived from the tensile strength of the material, f_t,

$$F_{n,max,contact\ i} = f_t\ A_{voronoi,contact\ i} \tag{11}$$

in which, $A_{voronoi,contact\ i}$ is the contact area given by the common inter-particle Laguerre Voronoi facet [26]. Based on the experimental results of Ward [20], the tensile strength of mortar and ITZ, and therefore each maximum normal contact force, were determined in order to reproduce the tensile strength of concrete. It was assumed that the tensile strength of ITZ was half of the mortar value and that the aggregate had 50% more tensile strength than the mortar (considering a good quality aggregate with higher ultimate properties), following results presented in [27]. Note that the maximum normal contact force is proportional to the contact area, which follows a distribution within the particle assembly. The distribution of maximum normal contact forces introduces a microstructural randomness into the model, representing areas with lower and higher strength values. Table 3.5 presents the minimum, mean and maximum normal contact forces for the particle assembly and for each concrete component.

Table 3.5: Adopted contact strength values

Material	f_t (MPa)	$A_{voronoi}$ (m²)			$F_{n,max}$ (kN)		
		Minimum value	Mean value	Maximum value	Minimum value	Mean value	Maximum value
Mortar	4	0.00064	0.00074	0.00096	2.6	3.0	3.8
ITZ	2				1.3	1.5	1.9
Aggregate	6				3.9	4.5	5.7

3.5.4 Effects of aging viscoelastic behaviour on the swelling development of the concrete specimen, considering damage

Regarding the same types of analysis as previously described but considering damage in each particle contact, the values of unbalance forces for each timestep and the total swelling, measured in one direction, at the end of the analysis also increase, due to internal damage and decrease of stiffness (Figures 3.9, 3.10 and 3.11). The differences between elastic and viscoelastic behaviour is more pronounced, with the viscoelastic behaviour resulting in lower total swelling due to lower damage. Damage has a significant effect on the total swelling of ASR-coarse agg. type analysis, when compared with the analysis without damage. Despite the small swelling areas inside the aggregates, the damaged areas have a great influence on the total swelling (Figure 3.11).

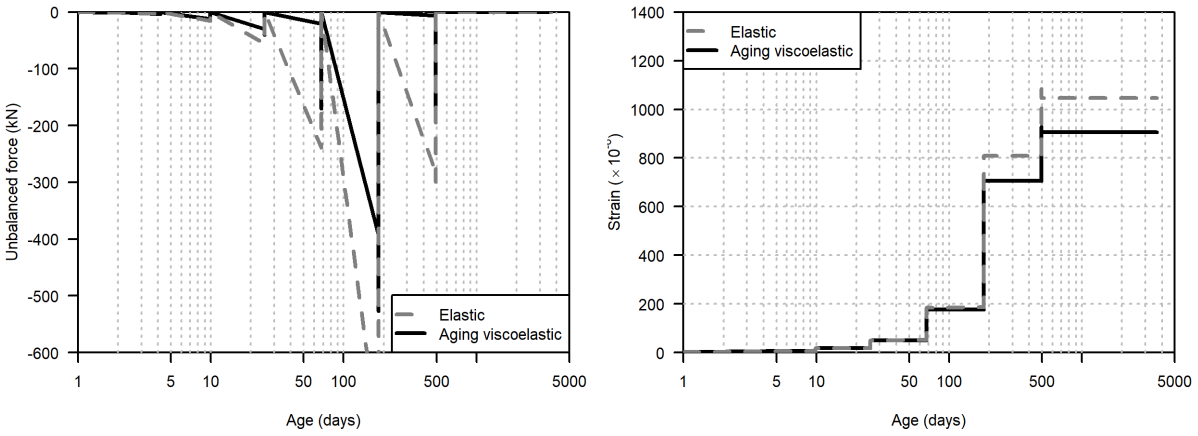

Figure 3.9: Development of unbalanced force during numerical test (left) and total swelling measured in one direction (right), for the ISR analysis, considering damage

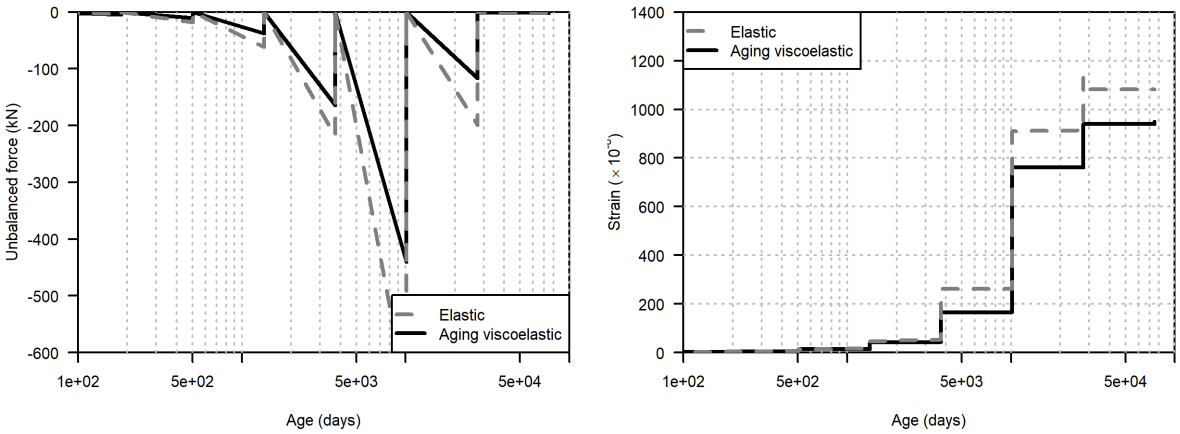

Figure 3.10: Development of unbalanced force during numerical test (left) and total swelling measured in one direction (right), for the ASR-fine agg. analysis, considering damage

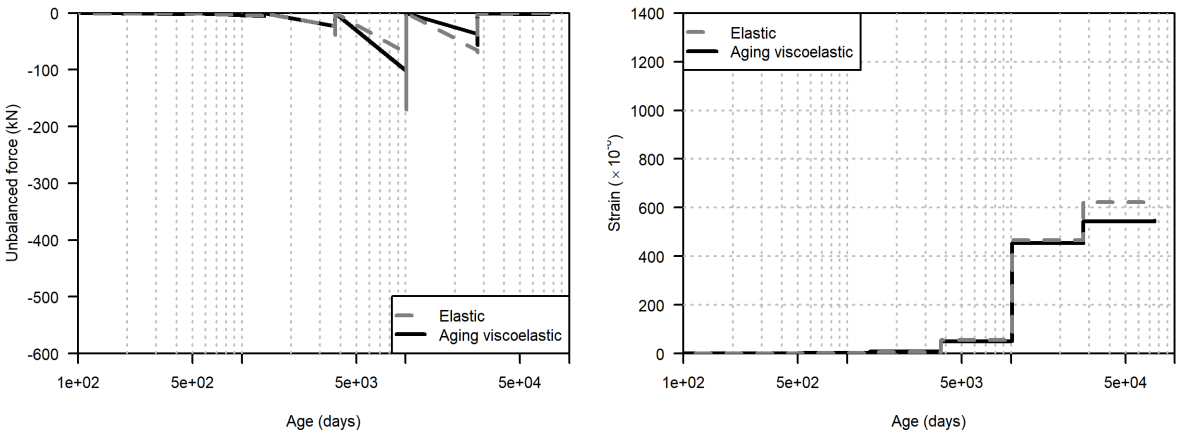

Figure 3.11: Development of unbalanced force during numerical test (left) and total swelling measured in one direction (right), for the ASR-coarse agg. analysis, considering damage

3.5.5 Effects of aging viscoelastic behaviour on the development of contact forces inside concrete, considering damage

Figures 3.12, 3.13 and 3.14 present the normal contact forces results of the simulation of a swelling test applied to a concrete particle model, considering damage of the binding mortar and the ITZ, for elastic and for aging viscoelastic behaviour and, for the ISR type analysis, for the ASR-fine agg. type analysis and for ASR-coarse agg. type analysis, respectively.

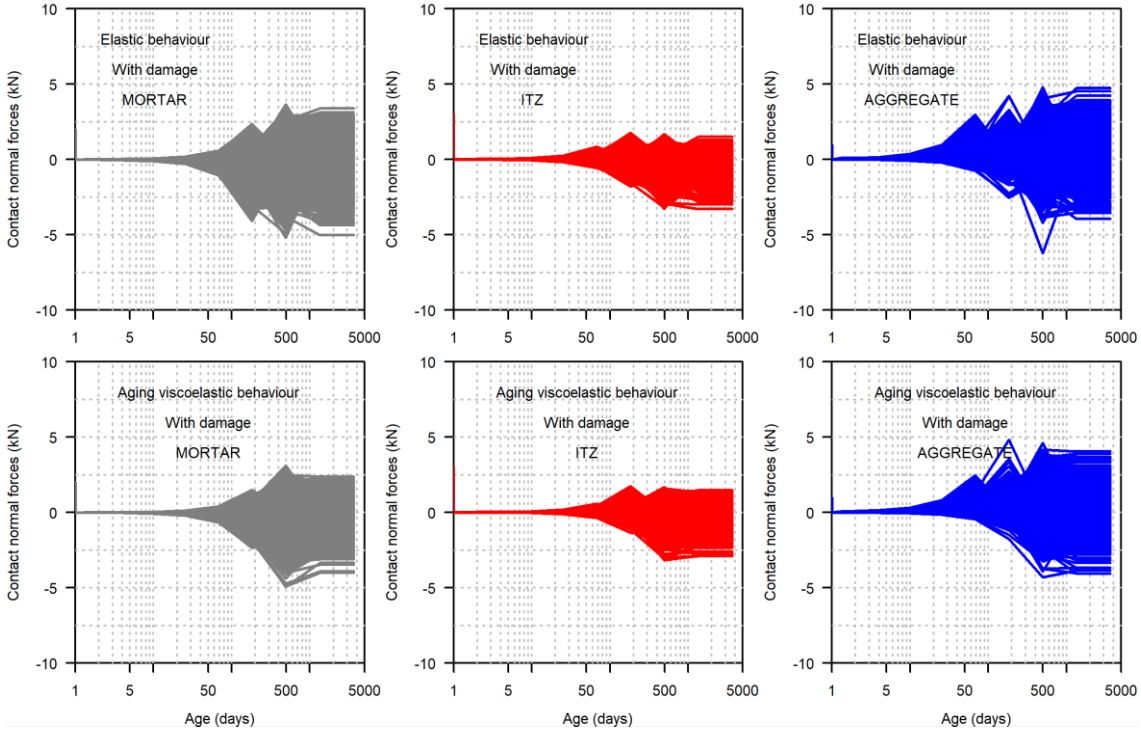

Figure 3.12: ISR type analysis results, considering damage: Normal contact forces development over time for each type of contact (mortar, ITZ and aggregate) considering elastic behaviour (top) and aging viscoelastic behaviour (bottom)

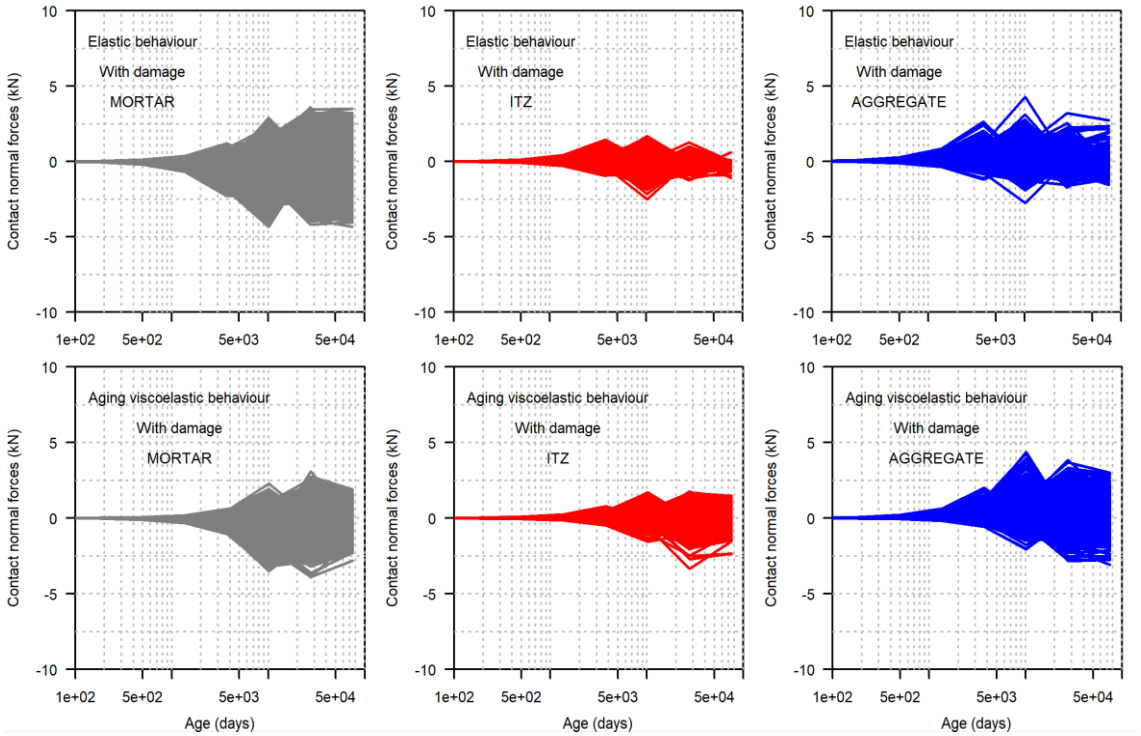

Figure 3.13: ASR-fine agg. type analysis results, considering damage: Normal contact forces development over time for each type of contact (mortar, ITZ and aggregate) considering elastic behaviour (top) and aging viscoelastic behaviour (bottom)

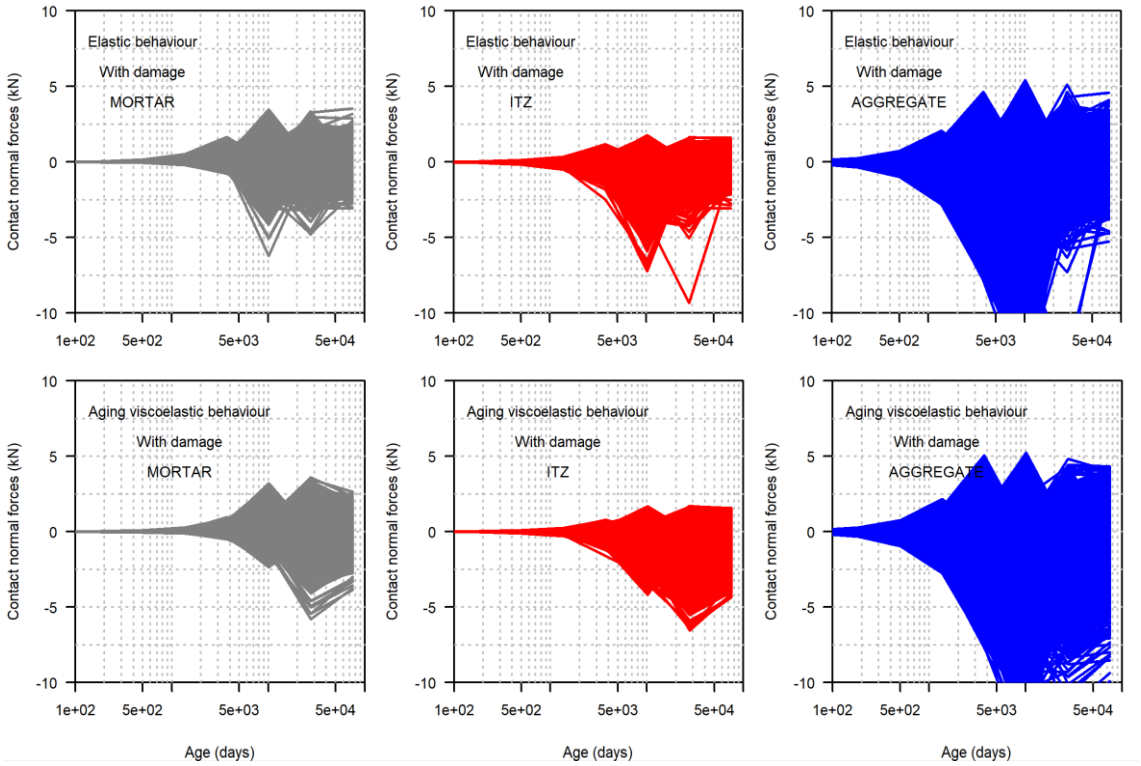

Figure 3.14: ASR-coarse agg. type analysis results, considering damage: Normal contact forces development over time for each type of contact (mortar, ITZ and aggregate) considering elastic behaviour (top) and aging viscoelastic behaviour (bottom)

Table 3.6 summarizes the obtained normal contact forces for each type of analysis considering damage, for each type of material. Numerical results show a reduction of normal compressive contact damage when aging viscoelasticity is taken into account for the mortar (27% for ISR and 56% for ASR-fine agg., in comparison with the reference, the elastic behaviour, Figure 3.12 and Figure 3.13). There was also a significant increase of the compressive forces on the ITZ contacts (75% for ISR and 280% for ASR-coarse agg.) and of the tensile forces on the aggregate contacts (220% for ISR) and a decrease of the tensile forces of the mortar (50% for ISR and 60% for ASR-fine agg.). An increase in the mortar and ITZ tensile forces was also noticed for the ASR-coarse agg. type analysis (125% and 200%, respectively) when considering the viscoelastic behaviour. This behaviour can be explained by the load transfer from the mortar and ITZ to the aggregates over time and by localization of cracks as damage progresses.

It was concluded that, at the intermediate ages, some damage is already visible around the aggregates but the internal forces in the mortar and in the aggregates have higher values than in the following timesteps. As damage progresses, the self-balanced forces inside the concrete dissipates and the aggregates are less likely to restrain the swelling increments which leads to less stress increments. Additionally, stress relaxation is taking place for each timestep in the remaining contacts.

Figure 3.15 compares the cracking patterns of the three types of analysis with a reported description of the literature [21]. It is shown that the proposed concrete particle model is able to represent the cracking patterns related to ISR (damage in the mortar and in the ITZ) and the cracking patterns related to ASR-coarse agg. (damage in the ITZ and damage in the larger aggregates). The obtained cracking patterns due to ASR-fine agg. are similar to the ISR patterns, with a large amount of damaged ITZ in comparison with the mortar. This can be due to the poor properties of the ITZ and high modulus of elasticity of the aggregates, which were considered the same for both analysis.

Table 3.6: Summary normal contact forces results of each analysis type, considering damage

Type of analysis	**Type of contact behaviour**	**Type of material**	**Normal contact forces (kN) | Variation to reference contact behaviour (%)**				**Normal contact damage (relative value) | Variation to reference contact behaviour (%)**	
			5%		**95%**			
ISR	Elastic (**reference**)	MORTAR	-1.5	-	1.4	-	2406 (12.4)	-
		ITZ	0.0	-	0.0	-	4568 (90.3)	-
		AGG	-0.4	-	0.5	-	1540 (16.2)	-
	Aging viscoelastic	MORTAR	-1-1	-27	0.7	-50	85 (0.4)	-96
		ITZ	-0.7	-	0.8	-	3456 (68.3)	-24
		AGG	-0.7	75	1.6	220	219 (2.3)	-86
ASR-fine agg.	Elastic (**reference**)	MORTAR	-1.6	-	1.5	-	2636 (13.6)	-
		ITZ	0.0	-	0.0	-	4980 (98.5)	-
		AGG	0.0	-	0.0	-	585 (6.2)	-
	Aging viscoelastic	MORTAR	-0.7	-56	0.6	-60	213 (1.1)	-92
		ITZ	-0.1	-	0.3	-	4346 (85.9)	-13
		AGG	-0.3	-	0.7	-	279 (2.9)	-52
ASR-coarse agg.	Elastic (**reference**)	MORTAR	-0.4	-	0.4	-	4128 (21.3)	-
		ITZ	-0.3	-	0.2	-	3107 (61.4)	-
		AGG	-0.5	-	0.5	-	2995 (31.5)	-
	Aging viscoelastic	MORTAR	-0.6	50	0.9	125	1492 (7.7)	-64
		ITZ	-1.4	367	0.6	200	1871 (37.0)	-40
		AGG	-1.9	280	1.1	120	2925 (30.8)	-2

Table 3.7 presents the result comparison of elastic behaviour without damage and aging viscoelastic behaviour with damage, for each type of analysis, highlighting the importance of these two phenomena on the prediction of concrete macroscopic behaviour, due to swelling. Overall, the aging viscoelastic behaviour yields a significant reduction of compressive and tensile forces in each concrete component. This effect seems to have a greater impact on the reduction of internal compressive forces (5% probability of contact force distribution).

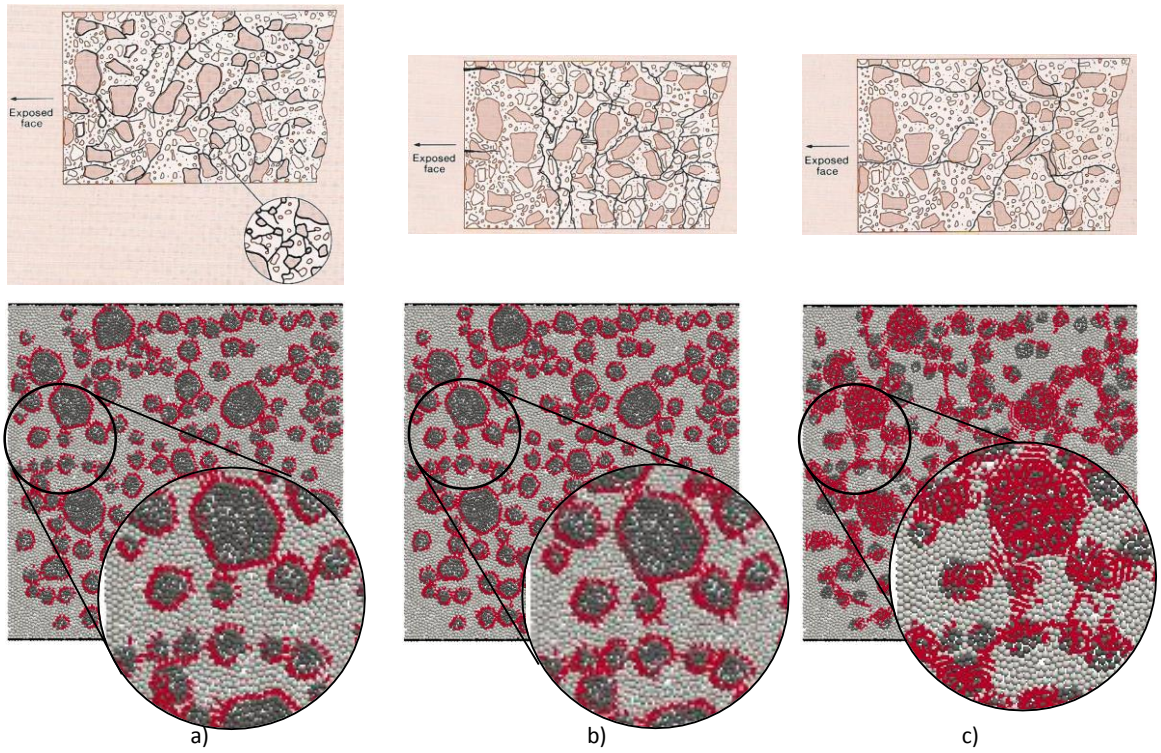

Figure 3.15: Comparison between internal cracking for each type of reactions, described in [21], (top line) and the analysis results, considering damage (general damage distribution (central line) and detailed damage distribution (bottom line)): a) ISR type; b) ASR-fine agg.; c) ASR-coarse agg.

Table 3.7: Comparison of normal contact forces results of each analysis type, considering elastic contact behaviour without damage and aging viscoelastic contact behaviour with damage

Type of analysis	**Type of contact behaviour**	**Type of material**	**Normal contact forces (kN) | Variation to reference contact behaviour (%)**				**Normal contact breaks (relative value)**
			5%		**95%**		
ISR	Elastic no damage (**reference**)	MORTAR	-8.3	-	2.5	-	0
		ITZ	-3.7	-	6.3	-	0
		AGG	0.0	-	8.4	-	0
	Aging viscoelastic no damage	MORTAR	-2.0	-76	0.6	-76	0
		ITZ	-1.6	-57	1.9	-70	0
		AGG	-0.5	-	3.1	-63	0
	Aging viscoelastic with damage	MORTAR	-1-1	-87	0.7	-72	85 (0.4)
		ITZ	-0.7	-81	0.8	-87	3456 (68.3)
		AGG	-0.7	-	1.6	-81	219 (2.3)
ASR-fine agg.	Elastic no damage (**reference**)	MORTAR	-13.5	-	3.8	-	0
		ITZ	-1.6	-	0.6	-	0
		AGG	0.5	-	1.2	-	0
	Aging viscoelastic no damage	MORTAR	-3.4	-75	1.0	-74	0
		ITZ	-0.7	-56	3.3	-69	0
		AGG	-0.2	-140	3.7	-67	0
	Aging viscoelastic with damage	MORTAR	-0.7	-95	0.6	-84	213 (1.1)
		ITZ	-0.1	-94	0.3	-97	4346 (85.9)
		AGG	-0.3	-160	0.7	-94	279 (2.9)
ASR-coarse agg.	Elastic no damage (**reference**)	MORTAR	-1.9	-	3.6	-	0
		ITZ	-8.6	-	4.6	-	0
		AGG	-55.4	-	30.7	-	0
	Aging viscoelastic no damage	MORTAR	-0.7	-63	1.1	-69	0
		ITZ	-3.2	-63	1.9	-59	0
		AGG	-47.7	-14	31.8	4	0
	Aging viscoelastic with damage	MORTAR	-0.6	-68	0.9	-75	1492 (7.7)
		ITZ	-1.4	-84	0.6	-87	1871 (37.0)
		AGG	-1.9	-97	1.1	-96	2925 (30.8)

4. CONCLUSIONS

This paper proposes and validates a swelling contact model for complex concrete particle models, considering the effect of both aging viscoelastic and damage behaviour. The aging viscoelastic behaviour of mortar and ITZ was taken into account based on previous work. The study focused on three types of swelling, ISR, ASR-fine agg. and ASR-coarse agg., in order to investigate the influence of aging viscoelasticity and damage on the development of internal contact forces for short-time and long-term analysis.

The results showed a significant reduction of compressive and tensile contact forces inside the concrete over time due to force relaxation. Force redistribution in the proposed particle model is also expected to occur due to stiffness increase of binding mortar and ITZ. It is shown that damage occurs mainly in the ITZ, considered to be a weaker area and enables other force redistribution and a progressively less restrained system.

The preliminary results that are presented show that particle models can be further used to the study of concrete swelling at the mesoscale, considering, for example, confinement and the presence of reinforcement, and have a great potential to be used in the modelling of mechanical property deterioration over time.

AKNOWLEDGEMENTS

The authors would like to thank Dr. António Santos Silva, Dr. Isabel Fernandes and Dr. João Custódio for their valuable insight on the origin of the different types of swelling and on the experimental evidence of swelling development at the mesoscale.

REFERENCES

1. Dunant CF, Scrivener KL (2010) Micro-mechanical modelling of alkali–silica-reaction-induced degradation using the AMIE framework. Cem Concr Res 40:517–525 . doi: 10.1016/j.cemconres.2009.07.024

2. Rajabipour F, Giannini E, Dunant C, et al (2015) Alkali–silica reaction: Current understanding of the reaction mechanisms and the knowledge gaps. Cem Concr Res 76:130–146 . doi: 10.1016/J.CEMCONRES.2015.05.024

3. Giorla AB, Scrivener KL, Dunant CF (2015) Influence of visco-elasticity on the stress development induced by alkali–silica reaction. Cem Concr Res 70:1–8 . doi: 10.1016/j.cemconres.2014.09.006

4. Saliba J, Grondin F, Matallah M, et al (2012) Relevance of a mesoscopic modeling for the coupling between creep and damage in concrete. Mech Time-Dependent Mater 17:481–499 . doi: 10.1007/s11043-012-9199-4

5. Briffaut M, Benboudjema F, Laborderie C, Torrenti JM (2013) Consequences of Internal Stresses Generated by Hydration on the Concrete Mechanical Behaviour. In: van Mier JGM, Ruiz G, Andrade C, et al (eds) FraMCoS-8 - VIII International Conference on Fracture of Concrete and Concrete Structures. Toledo, p 12

6. Xu Y, Xu Q, Chen S, Li X (2017) Self-restraint thermal stress in early-age concrete samples and its evaluation. Constr Build Mater 134:104–115 . doi: 10.1016/j.conbuildmat.2016.12.066

7. Scrivener KL, Crumbie AK, Laugesen P (2004) The interfacial transition zone (ITZ) between cement paste and aggregate in concrete. Interface Sci 12:411–421 . doi: 10.1023/B:INTS.0000042339.92990.4c

8. Saouma VE, Martin RA, Hariri-Ardebili MA, Katayama T (2015) A mathematical model for the kinetics of the alkali–silica chemical reaction. Cem Concr Res 68:184–195 . doi: 10.1016/j.cemconres.2014.10.021

9. Esposito R (2016) The Deteriorating Impact of Alkali-Silica Reaction on Concrete. Expansion and Mechanical Properties. PhD thesis. Delft University of Technology (TU Delft)

10. Cundall PA (1971) A computer model for simulating progressive large scale movements in blocky rock systems. In: International Society for Rock Mechanics (ed) Proceedings of the international symposium on rock fracture. Nancy, pp 129–136

11. Cundall PA, Strack ODL (1979) A discrete numerical model for granular assemblies. Géotechnique 29:47–65 . doi: 10.1680/geot.1979.29.1.47

12. Zubelewicz A, Mróz Z (1983) Numerical simulation of rock burst processes treated as problems of dynamic instability. Rock Mech Rock Eng 16:253–274 . doi: 10.1007/BF01042360

13. Plesha ME (1983) On the modeling of rocks with microstructure. In: 24th U.S. Symposium on Rock Mechanics. American Rock Mechanics Association, Station, Texas

14. Monteiro Azevedo N, Vieira de Lemos J, de Almeida JR (2008) Influence of aggregate deformation and contact behaviour on discrete particle modelling of fracture of concrete. Eng Fract Mech 75:1569–1586 . doi: 10.1016/j.engfracmech.2007.06.008

15. Alnaggar M, Cusatis G, Luzio G Di (2013) Lattice Discrete Particle Modeling (LDPM) of Alkali Silica Reaction (ASR) deterioration of concrete structures. Cem Concr Compos 41:45–59 . doi: 10.1016/j.cemconcomp.2013.04.015

16. Pan Y, Prado A, Porras R, et al (2017) Lattice Modeling of Early-Age Behavior of Structural Concrete. Materials (Basel) 10:231 . doi: 10.3390/ma10030231

17. Serra C, Azevedo NM, Lopes Batista A, Schclar N (2018) Discrete Element Method for Modeling the Long-Term Aging Viscoelastic Behavior of Concrete Considering Its Mesostructure. J Eng Mech 144: . doi: 10.1061/(ASCE)EM.1943-7889.0001434

18. Monteiro Azevedo N (2003) A rigid particle discrete element model for the fracture analysis of plain and reinforced concrete. PhD thesis. Heriot-Watt University

19. Larive C (1998) Apports combinés de l'expérimentation et de la modélisation à la compréhension de l'alcali-réaction et de ses effets mécaniques. LCPC - Laboratoire Central des Ponts et Chaussées, Paris

20. Ward M, Neville A, Singh S (1969) Creep of air-entrained concrete. Mag Concr Res 21:205–210 . doi: 10.1680/macr.1969.21.69.205

21. Sanchez LFM, Drimalas T, Fournier B, et al (2018) Comprehensive damage assessment in concrete affected by different internal swelling reaction (ISR) mechanisms. Cem Concr Res 107:284–303 . doi: 10.1016/J.CEMCONRES.2018.02.017

22. Esposito R, Hendriks MAN (2017) Literature review of modelling approaches for ASR in concrete: a new perspective. https://doi.org/101080/1964818920171347068 23:1311–1331 . doi: 10.1080/19648189.2017.1347068

23. Dunant CF, Scrivener KL (2012) Effects of aggregate size on alkali–silica-reaction induced expansion. Cem Concr Res 42:745–751 . doi: 10.1016/J.CEMCONRES.2012.02.012

24. Wang ZM, Kwan AKH, Chan HC (1999) Mesoscopic study of concrete I: generation of random aggregate structure and finite element mesh. Comput Struct 70:533–544 . doi: 10.1016/S0045-7949(98)00177-1

25. Bažant ZP, Baweja S (1995) Creep and shrinkage prediction model for analysis and design of concrete structures - model B3. Mater Struct 28:357–365

26. Candeias M, Monteiro Azevedo N, Braga Farinha L (2017) VGCM3D-A 3d rigid particle model for rock fracture following the Voronoi tessellation of the grain structure: formulation and validation. In: Wriggers P, Bischoff M, Oñate E, et al (eds) V International Conference on Particle-based Methods – Fundamentals and Applications. PARTICLES 2017. International Center for Numerical Methods in Engineering (CIMNE), Hannover, Germany, pp 99–110

27. Serra C (2018) Prediction of dam concrete structural properties based on wet-screened test results and mesoscale modelling. PhD thesis. Universidade Nova de Lisboa